Convective Cold Pools in Long-Term Boundary Layer Mast Observations

BASTIAN KIRSCH,[a] FELIX AMENT,[a] AND CATHY HOHENEGGER[b]

[a] *Meteorological Institute, University of Hamburg, Hamburg, Germany*
[b] *Max Planck Institute for Meteorology, Hamburg, Germany*

(Manuscript received 16 June 2020, in final form 15 December 2020)

ABSTRACT: Cold pools are mesoscale features that are key for understanding the organization of convection, but are insufficiently captured in conventional observations. This study conducts a statistical characterization of cold-pool passages observed at a 280-m-high boundary layer mast in Hamburg (Germany) and discusses factors controlling their signal strength. During 14 summer seasons 489 cold-pool events are identified from rapid temperature drops below −2 K associated with rainfall. The cold-pool activity exhibits distinct annual and diurnal cycles peaking in July and midafternoon, respectively. The median temperature perturbation is −3.3 K at 2-m height and weakens above. Also the increase in hydrostatic air pressure and specific humidity is largest near the surface. Extrapolation of the vertically weakening pressure signal suggests a characteristic cold-pool depth of about 750 m. Disturbances in the horizontal and vertical wind speed components document a lifting-induced circulation of air masses prior to the approaching cold-pool front. According to a correlation analysis, the near-surface temperature perturbation is more strongly controlled by the pre-event saturation deficit ($r = -0.71$) than by the event-accumulated rainfall amount ($r = -0.35$). Simulating the observed temperature drops as idealized wet-bulb processes suggests that evaporative cooling alone explains 64% of the variability in cold-pool strength. This number increases to 92% for cases that are not affected by advection of midtropospheric low-Θ_e air masses under convective downdrafts.

SIGNIFICANCE STATEMENT: Cold pools are areas of cool and dense air underneath precipitating clouds that often trigger new convection as they spread outward. Although cold pools are key for correctly representing convection in numerical simulations, their observational characterization is insufficient, focusing on few cases and surface measurements. We analyze meteorological observations of nearly 500 cold-pool passages sampled during 14 years at a 280-m-high mast in Hamburg (Germany). The robust data basis shows that the typical temperature perturbation associated with cold pools is only −3.3 K and weakens with height. The surface temperature signal is mainly driven by evaporative cooling of below-cloud air by rainfall, whereby the saturation deficit is a much better predictor than the often used precipitation amount.

KEYWORDS: Convective-scale processes; Cold pools; In situ atmospheric observations; Updrafts/downdrafts; Evaporation

1. Introduction

Cold pools are mesoscale areas of cool downdraft air that form through evaporation underneath precipitating clouds. The importance of cold pools for the variability of convective precipitation is a long-standing topic in the literature. Many studies have described a variety of dynamical and thermodynamical processes that relate cold pools to the formation and organization of convection. As the negatively buoyant air of a cold pool horizontally propagates on Earth's surface as a density current, its leading edge represents a preferred region for the initiation of secondary convection. While one factor is the mechanical lifting of less dense air ahead of the cold-pool front, the interplay between cold pools and vertical wind shear also has a strong impact on the organization and hence life cycle of convective squall lines (Rotunno et al. 1988; Grant et al. 2018). Furthermore, the modification of the near-surface moisture field by cold pools is thought to be important for the life cycle of convection. Studies on numerical simulations of oceanic cold pools identified their leading edge as a region of enhanced moisture in the lower troposphere, where secondary updrafts are preferably triggered (e.g., Tompkins 2001; Feng et al. 2015; Torri et al. 2015). However, those cold-pool moisture rings are rarely found in observational data (De Szoeke et al. 2017; Chandra et al. 2018) and their primary origin is still under debate (Langhans and Romps 2015; Schlemmer and Hohenegger 2016; Zuidema et al. 2017).

Khairoutdinov and Randall (2006) proposed that cold pools particularly favor the transition from shallow to deep convection, since they support the formation of large convective clusters that are less affected by entrainment of drier environmental air. In this context, Schlemmer and Hohenegger (2014), Schlemmer and Hohenegger (2016), and Haerter and Schlemmer (2018) argued that the modification of surface fluxes and moisture fields by cold pools supports this positive feedback loop and the subsequent organization of convective clouds into larger clusters. As a consequence, the representation of cold-pool characteristics and dynamics is a critical component for correctly simulating the diurnal cycle of precipitation (Rio et al. 2009; Boeing et al. 2012; Kurowski et al. 2018).

Corresponding author: Bastian Kirsch, bastian.kirsch@uni-hamburg.de

DOI: 10.1175/MWR-D-20-0197.1

© 2021 American Meteorological Society. For information regarding reuse of this content and general copyright information, consult the AMS Copyright Policy (www.ametsoc.org/PUBSReuseLicenses).
Brought to you by MAX-PLANCK-INSTITUTE FOR METEOROLOGY | Unauthenticated | Downloaded 04/15/21 07:31 AM UTC

Cold pools are short-lived phenomena that lead to rapid perturbations in various meteorological parameters. A large number of studies have investigated cold-pool characteristics based on model simulations with a spatial resolution of <1 km. Such simulations are able to explicitly resolve the scale of convective clouds. However, observational evidence is essential for validating simulated cold-pool properties and related processes. Several observational studies have aimed to characterize the signal of cold pools in different climatological conditions. In the analysis of selected outflow passages in tower measurement data in Oklahoma, Goff (1976) found a sequence of typical disturbances in meteorological parameters for different thunderstorm life cycle stages. This includes a mean hydrostatic pressure rise of 2.5 hPa, followed by wind gusts of 12.8 m s^{-1} associated with a rapid shift in wind direction and a potential temperature drop of 4.3 K, occurring within 35 min prior to the onset of rainfall. Engerer et al. (2008) reported pressure increases between 3.2 and 4.5 hPa, potential temperature deficits between 5.4 and 11 K and wind gusts of at least 15 m s^{-1} associated with the passage of outflows from mesoscale convective system (MCS) storms as seen in Oklahoma Mesonet stations. Similar analyses for locations in northern Africa can be found in Redl et al. (2015) and Provod et al. (2016). Furthermore, there exists strong observational evidence for generally much weaker signals of cold pools forming in tropical oceanic environments compared to continental midlatitude conditions (Terai and Wood 2013; Feng et al. 2015; De Szoeke et al. 2017; Vogel 2017).

There have also been numerous efforts to identify factors controlling the thermodynamical properties of cold pools. In an early study, Fujita (1959) assigned the cold-air production to evaporation of precipitation in mesoscale thunderstorm systems based on surface and airborne observations over several locations in the United States. He found the total density increase by evaporation in the subcloud layer and the associated hydrostatic pressure rise to be proportional to the surface rainfall. Barnes and Garstang (1982) used radar and in situ measurements over the tropical Atlantic to derive a precipitation threshold of 2 mm h^{-1} to distinguish between nonpenetrative downdrafts that are associated with light rainfall and mainly cool and moisten the subcloud layer, and penetrative downdrafts that rain heavily and import lower moist static energy from above cloud base into the surface layer. By affecting evaporative cooling and the characteristics of downdraft air masses, the atmospheric profile critically affects the strength of a cold pool. Warm and dry boundary layers support strong cooling rates by rain evaporation, which is usually more important for continental convection. The relationship between cold-pool strength and midtropospheric conditions is less straightforward. Dry air supports the formation of downdrafts through entrainment and subsequent evaporation of midlevel air, which tends to strengthen updrafts and increase the condensate mass available for evaporation (Markowski and Richardson 2010; Böeing et al. 2012; Feng et al. 2015). The actual evaporative cooling also depends on the type of hydrometeors, e.g., rain versus ice particles, which in turn strongly depends on the present thermodynamical conditions (Engerer et al. 2008; Li et al. 2015). Turbulent mixing of environmental air into the cold pool and erosion by surface heat fluxes finally contribute to its dissipation (Ross et al. 2004; Gentine et al. 2016; Grant and van den Heever 2016, 2018).

Considering the variety and complexity of parameters acting on the thermodynamics of cold pools, the identification of dominant processes determining their observed properties is a challenging task that has not been satisfactorily addressed yet. In the present study we use a multiyear observational dataset to provide a robust characterization of continental cold pools. Unlike existing studies, we do not restrict our analysis to preselected events from specific types of convection, which tend to be biased toward strong and less frequent events, but include cold pools from a wide range of meteorological conditions. Furthermore, we aim to quantitatively estimate the relevance of the prevailing atmospheric conditions for explaining the observed variability in the near-surface temperature signal and disentangle the impact of evaporative cooling and convective import of upper-level air masses. The presented results could serve as a reference dataset for modeled cold-pool properties in state-of-the-art large-eddy simulations (LES) and provide guidance for the identification of potential model biases. The study is structured as follows: after introducing the used dataset and applied method for cold-pool identification in section 2, we discuss the signal characteristics of the observed events in section 3. In section 4 we focus on the factors controlling the cold-pool strength, followed by a summary of the overall findings in section 5.

2. Data and methodology

a. Observational dataset

This study analyzes meteorological observation data from the Hamburg weather mast boundary layer tower in Hamburg (Germany). The measurement facility is installed at a television broadcasting tower located in the eastern outskirts of the city (53.5192°N, 10.1029°E). The 305-m-high main mast is equipped with instrumentation at platforms in six different heights, while near-surface measurements are conducted at a 12-m mast located in 170-m distance on a nearby meadow. The instrumentation of the main mast relevant for the present study consists of platinum resistance thermometers (Pt-100), HMP 45 humidity sensors and 3D ultrasonic anemometers, while the near-surface observations are accomplished by PTB 200 A pressure sensors and a tipping-bucket rain gauge. All measurements are available at 1-min temporal resolution. A more detailed description of the measurement site and instrumentation can be found in Brümmer et al. (2012).

For the present analysis we use observational data from 14 summer seasons (1 April to 30 September) between 2006 and 2019 from five height levels (2, 50, 110, 175, and 280 m), while the lowest wind speed measurements refer to 10-m height. For years before 2011 the topmost available measurement height is 250 m. Since air pressure is only recorded at the surface, we calculate its values at the four upper levels from the respective temperature data by applying the hydrostatic equation

Brought to you by MAX-PLANCK-INSTITUTE FOR METEOROLOGY | Unauthenticated | Downloaded 04/15/21 07:31 AM UTC

between the observed heights. These pressure values also go into the calculation of the equivalent potential temperature after Bolton (1980), which we mainly use to interpret controls on cold-pool properties.

b. Detection and definition of cold-pool events

The investigation of observed cold-pool characteristics first requires the identification of their footprints in local meteorological parameters. Since a subjective identification of single cold-pool events in multiyear data is unfeasible, we apply an objective detection method based on simple threshold criteria (Kirsch 2020). To minimize the influence of prescribed constraints on our results, the algorithm only takes 2-m air temperature T_2 and rainfall rate R as input parameters. For the identification of cold-pool-related signals in the measurement records, the algorithm scans the input temperature time series for a difference of $\Delta T_2 \leq -2$ K within 20 min after the current time step. The first of the subsequent time steps satisfying a temperature decrease of at least 0.5 K then defines the beginning of the cold-pool event, denoted by t_0. Subsequent decreases in temperature within the following 60 min are considered to be part of the same event. To attribute the detected temperature drops to the passage of a convectively driven cold pool rather than local meteorological effects, identified events without rainfall within 1 h after t_0 are excluded. The same is true for very rare events that include missing values either in the temperature or rainfall record from 30 min before to 60 min after t_0.

The detection method identifies an overall number of 489 temperature drops satisfying the applied criteria. We consider the discussed results as statistically representative, since the temperature data availability per summer season is always larger than 95.3% and above 99% in 11 out of 14 years. As the applied cold-pool-detection algorithm is only based on the local temperature and rainfall record and does not use any information about the origin of the identified temperature drops, the results are potentially affected by the misinterpretation of synoptic-scale cold-frontal passages as local-scale cold-pool events. The manual inspection of 6-hourly surface analysis charts (Deutscher Wetterdienst 2019) for 2017 and 2018, representing years with a very high and very low number of identified events, shows that 20.5% and 11.5% of the detected events occurred within a time range of 2 h before or after a cold-front passage, respectively. Still these events might not have been directly caused by the cold front itself, but rather by prefrontal convection or convective cells embedded into the front.

For a coherent description of short-term meteorological signals during a cold-pool-front passage, we consider a unified analysis scheme for the different variables. To calculate the signal strength in each variable, we first define its unperturbed state as the median value of the 30-min period prior to the detected begin of the event t_0, which is more robust against the imprecise timing of t_0 than taking the arithmetic mean. The signal strength is then given by the difference between this unperturbed state and the extreme value within 60 min after t_0. According to the sign of the respective signal, we define the extreme value as the minimum value for temperature T and equivalent potential temperature Θ_e and the maximum value for air pressure p, specific humidity q, horizontal wind speed U, and vertical wind speed w. In the case of w, the maximum value refers to the entire 90-min period to include also signals prior to the cold-pool-front passage. For each event, the same t_0 is used for all measurement heights and variables. Missing observations of p, q, or U slightly reduce the number of cases considered in the analysis to at least 448 of the 489 detected cases. The data for w only includes between 216 and 245 cases, as the variable was not measured before 2013.

3. Observed cold-pool characteristics

a. Frequency of events

As the first step to analyze the observed cold pools, we determine the frequency and occurrence of events. The annual number of events exhibits a large variability with a mean of 34.9 ± 6.8 events (Fig. 1a); however, the cold-pool activity follows a distinct annual cycle peaking in July (7.6 events per month) and a sharp weakening toward the end of the summer season in September (3.2 events per month; Fig. 1b). Furthermore, cold pools mainly occur during the second half of the day with a pronounced frequency peak at 1500 local time (Fig. 1c). These statistics confirm that the detected temperature drops are tightly connected to convective activity, as expected. The observed diurnal cycle in cold-pool frequency with a distinct minimum in the early morning hours also proves a lack of contamination of the presented results by synoptic-scale cold fronts.

b. Strength and temporal evolution of signal

We further characterize the observed properties of cold pools by studying the frequency distributions of the detected signals (Fig. 2) and the mean time series during the events (Fig. 3). Figure 2a indicates that the 2-m temperature perturbation ΔT_2 exhibits a median of −3.3 K and a minimum value of −10.8 K. As expected, the magnitude of the values is by several kelvins smaller than the ones reported by Engerer et al. (2008), who only included cases from MCS storms into their analysis. Width and skewness of the distribution is similar between the different measurement heights; however, the median signal strength constantly weakens with height to −2.4 K at 280 m. From the weakening temperature signal we can conclude that the temperature inside the cold-pool air generally decreases less strongly with height than outside of it. Therefore, we find evidence for an increased atmospheric stability within a cold pool compared to its surrounding. According to Fig. 3a, ΔT generally exhibits its largest gradient to the surrounding within 15 min after t_0. The early onset of the temperature drop a few minutes before t_0 results from the chosen thresholds to define a cold-pool event. After the strongest perturbation is reached 20–25 min after t_0, the temperature only recovers marginally, since a large fraction of the recorded events occurred after the diurnal maximum of solar heating. Moreover, this slow recovery could also indicate that the cold pool is still passing over the

Brought to you by MAX-PLANCK-INSTITUTE FOR METEOROLOGY | Unauthenticated | Downloaded 04/15/21 07:31 AM UTC

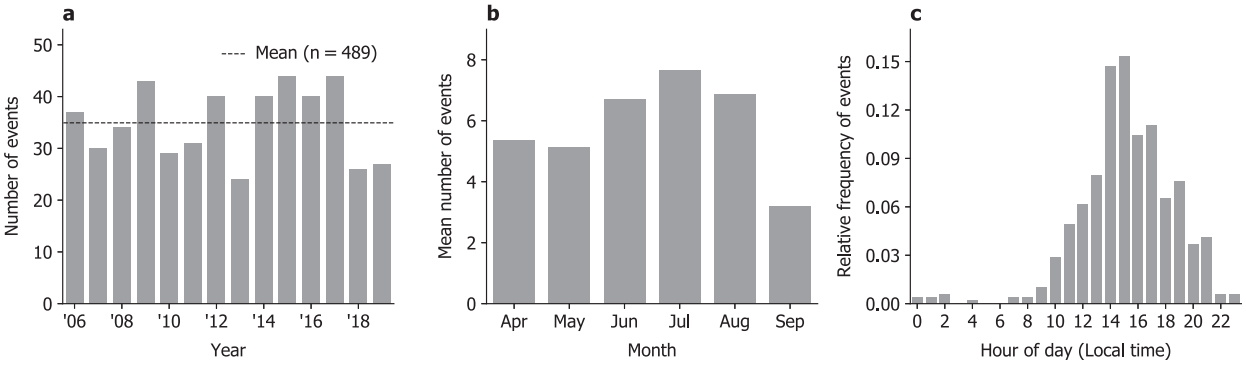

FIG. 1. Occurrence of cold-pool events detected at Hamburg weather mast between 2006 and 2019: (a) number of events per summer season (1 Apr–30 Sep), (b) mean annual cycle, and (c) mean diurnal cycle.

measurement site, even 1 h after its arrival. With a typical advection velocity of 10 m s^{-1}, this would imply a cold-pool size of 30 to 40 km, which could also be potentially observed in operational station networks.

The pressure signal Δp_2 is mostly confined to ≤2 hPa, while extreme cases of up to 5.9 hPa are observed (Fig. 2b). These values are by more than a factor of 2 smaller than for MCS-type cold pools as found by Engerer et al. (2008). Similar to the temperature signal, also Δp constantly decreases with height from a median of 0.7 hPa near the surface to 0.5 hPa at the uppermost height, as a direct result of the hydrostatic relationship employed to infer p at higher levels. The onset of Δp starts approximately 15 min earlier than that of ΔT (Fig. 3b), which is in line with the findings of other authors (Goff 1976; Engerer et al. 2008). The slight decline in pressure excess about 15 min after t_0 may be a sign of the partially nonhydrostatic nature of the initial perturbation due to dynamical effects at the propagating cold-air boundary (Houze 1993; Markowski and Richardson 2010). The importance of nonhydrostatic effects for the observed pressure signal during cold-pool events would require further investigation, which is beyond the scope of this study.

The majority of observed cold-pool passages leads to an moistening of the air, as shown in Figs. 2c and 3c. Based on a median of 1 g kg^{-1} near the surface and approximately 0.6 g kg^{-1} at 280 m above ground, Δq indicates a slight weakening of the moistening with height; however, magnitude and even sign of the signal are highly variable throughout all

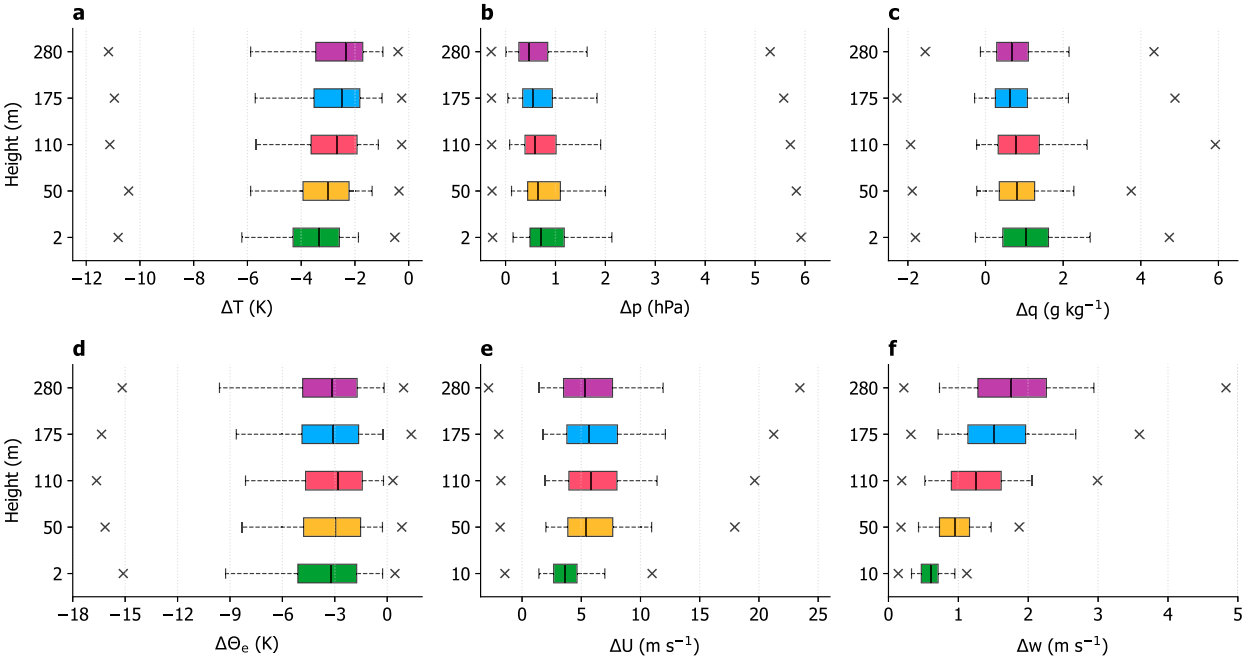

FIG. 2. Height-dependent distributions of perturbations in (a) air temperature T, (b) pressure p, (c) specific humidity q, (d) equivalent potential temperature Θ_e, (e) horizontal wind speed U, and (f) vertical wind speed w during cold-pool passages at Hamburg weather mast between 2006 and 2019. Vertical lines, boxes, and whiskers represent median, interquartile range, and 5% and 95% quantiles, respectively, while crosses mark the extreme values.

Brought to you by MAX-PLANCK-INSTITUTE FOR METEOROLOGY | Unauthenticated | Downloaded 04/15/21 07:31 AM UTC

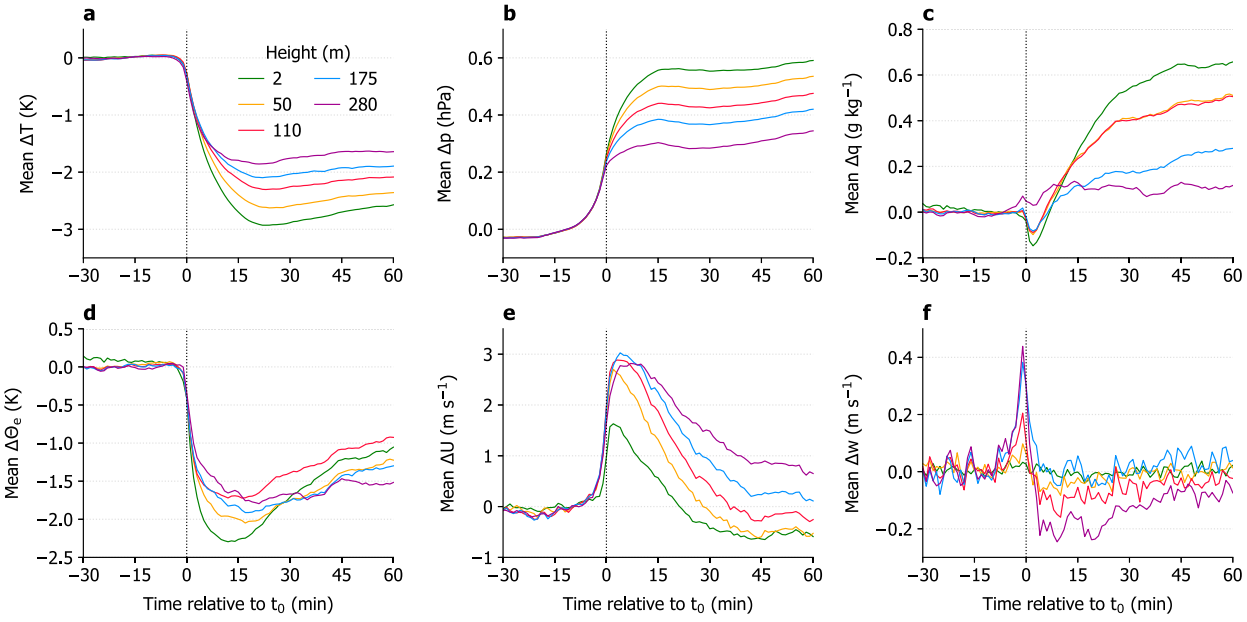

FIG. 3. As in Fig. 2, but for the mean temporal evolution of the quantities relative to the detected cold-pool-front passage t_0.

observation heights. For the present definition of Δq, i.e., using the difference between the unperturbed state and the maximum postpassage value, about 10% of the cases even show a decrease in humidity. This number increases to about 25%, if the median value of q within 60 min after the passage would be considered to calculate Δq. The large variability in Δq most likely reflects the interplay of different cold-pool-formation processes, namely evaporation, that would moisten the cold pool, and convective import of upper-layer air masses that would dry it. This interplay is discussed in section 4. However, a clear moisture ring along the cold-pool edge, as reported from numerical simulations, is not visible. The difficulty in observing a moisture ring is consistent with past observational studies, which have revealed inconsistencies in magnitude and sign of the cold-pool moisture signal in different climatic regimes (Feng et al. 2015; Redl et al. 2015; Provod et al. 2016; De Szoeke et al. 2017; Vogel 2017). The weak temporary dip in Δq just after t_0 in Fig. 3c is not of physical nature, but an instrumental artifact of the humidity sensor used before 2018 and relates to a longer response time compared to the temperature sensor. Most likely this issue also explains the longer equilibration time of the Δq signal compared to ΔT and Δp.

Combining the effects of temperature and humidity, also the perturbation in equivalent potential temperature $\Delta\Theta_e$ gives insights into properties of the observed cold pools (Figs. 2d and 3d). Similar to ΔT, the near-surface perturbation in Θ_e exhibits a median of −3.2 K and much larger extreme values of up to −15 K. However, $\Delta\Theta_e$ does not significantly vary with height. Since the pre-event Θ_e is also generally uniform with height (not shown), this suggests that Θ_e inside the cold pool does not significantly vary with height either. From this we conclude that the horizontal mixing between cold pool and environmental air throughout the lowest 280 m of the atmosphere is generally very limited. The steeper time derivative in $\Delta\Theta_e$ just after the detected cold-pool passage compared to ΔT also results from the same instrumental artifact in the measurement of q, as already discussed.

Finally, the passage of a cold-pool front goes along with a significant disturbance of the local wind field. The mean temporal evolution of ΔU indicates a distinct peak in horizontal wind speed just after t_0 throughout all heights (Fig. 3e). ΔU exhibits a median of 3.6 m s^{-1} at 10 m, while this value increases to 5.4 m s^{-1} at 50 m, but stays almost constant above (Fig. 2e). Only for extreme cases ΔU continuously increases with height from 11.0 m s^{-1} near the surface to 23.5 m s^{-1} at the top of the mast. The profile of ΔU as well as the constantly increasing width of the peak with height result from the deceleration of wind gusts close to the surface by friction. The mean time series of the perturbation in vertical wind speed Δw shows a distinct and short-lived peak shortly before the detected passage of the cold-pool front (Fig. 3f). Since the amplitude of the peak clearly exceeds the turbulence-induced noise level, it is indicative for a laminar flow feature that is consistently present throughout a large number of events. In combination with the following period of negative perturbations, this signature clearly marks the lifting of air masses prior to the arriving cold-pool air with compensating subsidence afterward. In contrast to ΔU, both the median of Δw (Δw_{10} = 0.6 m s^{-1}, Δw_{280} = 1.8 m s^{-1}) and its maximum values constantly increase with height, which marks a stronger lifting of air masses aloft (Fig. 2f). In summary, the coherent signals of ΔU and Δw suggest the presence of a lifting-induced overturning circulation ahead of the cold-pool front.

c. *Cold-pool depth*

Consistent with early studies on the vertical structure of convective cold air outflows (e.g., Fujita 1959; Barnes and Garstang 1982), our results in section 3b confirm the strongest

Brought to you by MAX-PLANCK-INSTITUTE FOR METEOROLOGY | Unauthenticated | Downloaded 04/15/21 07:31 AM UTC

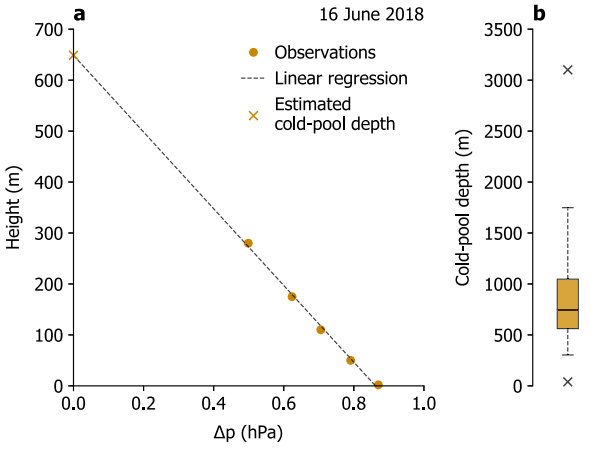

FIG. 4. (a) Height-dependent pressure perturbation Δp for a cold-pool event on 16 Jun 2018 and linear extrapolation for estimation of cold-pool depth and (b) distribution of estimated cold-pool depth for all cases between 2006 and 2019 that satisfy the linear model and yield depths >4 km. Horizontal line, box, and whiskers represent the median, interquartile range, and the 5% and 95% quantiles, respectively, while crosses mark the extreme values.

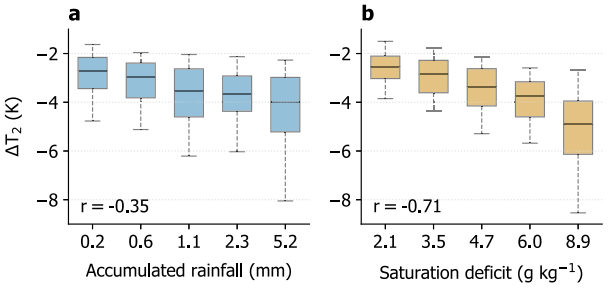

FIG. 5. Distribution of cold-pool 2-m air temperature perturbation ΔT_2 dependent on (a) event-accumulated rainfall and (b) pre-event median saturation deficit $q_{sat} - q$. Boxplots use 20% quantile interval bins labeled with the median values of each bin. Vertical lines, boxes, and whiskers mark the median, interquartile range, and the 5% and 95% quantiles, respectively. The linear correlation coefficient r indicated in (a) is calculated between the logarithmic rainfall amount and ΔT_2.

thermodynamical signal of a cold pool to be near the surface and to constantly weaken with height. We use the information of vertical gradients to infer the depth of individual cold pools. According to the hydrostatic relationship, the perturbation in air pressure Δp induced by the additional weight of the dense cold-pool air decreases approximately linearly with height. Therefore, the linear extrapolation of this gradient to the height where Δp vanishes provides an estimate of the cold-pool depth (Fig. 4a). We apply this method to cold-pool events that exhibit positive pressure perturbations for all measurement heights and satisfy the linear relationship between Δp and height according to an overall correlation coefficient of at least 0.95 for the entire profile. Furthermore, we neglect three cases for which the method yields unrealistically large (>4 km) values. A potential source of uncertainty might be the fact that the pressure signal is measured only at surface level and hydrostatically calculated from the respective temperature profile for the levels above. Figure 4b illustrates the resulting frequency distribution of cold-pool depths for 419 valid cases, showing an estimated depth of between a few hundred meters and almost 2000 m for most events and a median of 746 m. This result is in good agreement with Markowski and Richardson (2010), who reported a typical depth of 1 km for continental convective outflows. In contrast, corresponding values for tropical oceanic outflows are substantially smaller (<500 m), consistent with the lower cloud-base height (Terai and Wood 2013; De Szoeke et al. 2017).

4. Factors controlling the cold-pool strength

The results discussed in section 3 illustrate the distinct footprint of observed cold-pool passages in various meteorological parameters. However, the cold-pool characteristics also largely vary case-to-case from the average, e.g., reflected by the temperature perturbation ΔT ranging between −2 K and almost −11 K. Since the surface temperature signal of a convective outflow is indicative of its mass excess and, therefore, its potential to propagate and induce secondary convection, the explanation of its variability is an important step toward an improved understanding of convective organization. Based on the present observational dataset we aim to identify the main factors controlling the observed cold-pool strength. In our analyses we consider the strength of cold pools solely in terms of temperature perturbation ΔT.

a. Observational evidence

To investigate the variability in cold-pool strength, we first quantify its observed degree of relation with potential controlling factors. As a first approximation we assume cold pools to be mainly formed by evaporation underneath precipitating clouds and expect ΔT to be determined by the amount of rainwater in the subcloud layer available for evaporation. Figure 5a shows the distribution of ΔT as a function of the accumulated rainfall amount measured during the 90-min reference period of the cold-pool event. Although the median strength constantly increases from −2.7 K for weak-precipitation events to −4.0 K for strong-precipitation events, the linear correlation is weak (correlation coefficient $r = -0.35$). One reason for this weak relationship might be the poor representativeness of a surface rainfall point measurement. However, the inclusion of radar-based spatially distributed rainfall information does not significantly change the result (not shown).

The second relevant factor in controlling the degree of cooling by rainfall is the evaporation potential of the subcloud layer air. We quantify the potential for evaporative cooling via the absolute saturation deficit, which is given by the difference between saturation specific humidity q_{sat} and specific humidity q and mainly depends on the temperature and humidity of the given air mass. This quantity can be considered as independent from the rainfall amount, since both factors are practically uncorrelated ($r = 0.05$). As Fig. 5b shows, ΔT has a stronger dependence on the pre-event saturation deficit than on the accumulated rainfall ($r = -0.71$). The amplification of

Brought to you by MAX-PLANCK-INSTITUTE FOR METEOROLOGY | Unauthenticated | Downloaded 04/15/21 07:31 AM UTC

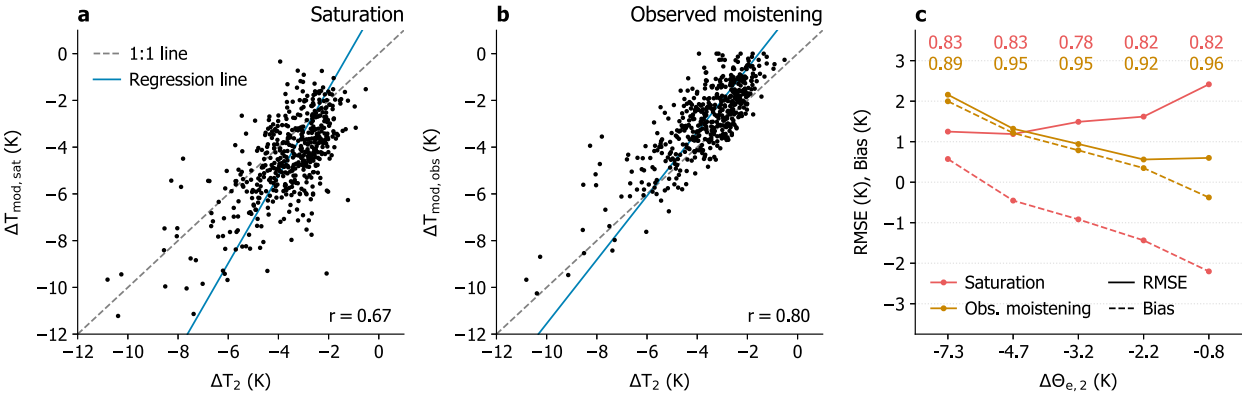

FIG. 6. Relationship between observed 2-m air temperature perturbation ΔT_2 and modeled temperature perturbations (a) $\Delta T_{\mathrm{mod,sat}}$ and (b) $\Delta T_{\mathrm{mod,obs}}$, corresponding to evaporative cooling until saturation and maximum relative humidity observed after the cold-pool passage is reached, respectively. (c) Root-mean-square error, bias, and linear correlation coefficient r (indicated as numbers) for both cases as a function of observed 2-m equivalent potential temperature perturbation $\Delta\Theta_{e,2}$, binned in 20% quantile intervals and labeled with the median values of each bin.

cold-pool strength with increasing saturation deficit is especially striking for the 20% most undersaturated cases that exhibit a median temperature deficit of −4.9 K. These results provide observational evidence that both the amount of rainfall and the evaporation potential of the pre-event air actually control the strength of the cold-pool temperature signal, with the latter being the more important one.

b. *Role of evaporation*

We further explore the importance of evaporative cooling for the observed cold-pool strength by simulating it in a simple thermodynamical model. In this model we assume that evaporation of rainfall cools and moistens an air parcel in the subcloud layer according to the wet-bulb process. When liquid water of mass Δm_W adiabatically and isobarically evaporates at the expense of the thermal energy of the air parcel, then its temperature approximately changes by

$$\Delta T \approx -\frac{L_v}{c_p}\,\Delta r_v. \tag{1}$$

Accordingly, the water vapor mixing ratio r_v increases by $\Delta r_v = \Delta m_w/m_a$, where m_a denotes the mass of dry air. L_v and c_p are the latent heat of evaporation of water and the specific heat capacity of dry air, respectively, whereas we neglect the change in specific heat capacity due to the increase in humidity.

For each cold-pool event we initialize the model with the observed pre-event temperature and relative humidity and let rainwater evaporate until the air mass reaches an equilibrium state. We define two equilibrium states of the model: first, the maximum wet-bulb temperature depression $\Delta T_{\mathrm{mod,sat}}$, where the considered air parcel cools and moistens until saturation is reached; second, the temperature depression $\Delta T_{\mathrm{mod,obs}}$ that denotes the state when the simulated relative humidity reaches the maximum value that was actually observed after the respective cold-pool passage, allowing for a more realistic undersaturated state. Since the cooling of the air parcel during the wet-bulb process also reduces its saturation vapor pressure and again impacts the moistening required to reach the respective equilibrium states, we cannot solve Eq. (1) directly. To realistically simulate this process we iteratively increase r_v by sufficiently small increments $\Delta r_{v,i} \approx 10^{-6}\,\mathrm{kg\,kg^{-1}}$ and adjust temperature and humidity of the air parcel accordingly.

The statistical analysis in Fig. 6a shows a reasonable agreement between the observed ΔT and its modeled values of maximum evaporative cooling $\Delta T_{\mathrm{mod,sat}}$ with a correlation coefficient of $r = 0.67$ and a root-mean-square error (RMSE) of 1.7 K. In this configuration the simple model tends to overestimate the cold-pool strength, especially for strong events. This indicates that in most cases the pre-cold-pool air is not moistened to saturation and, therefore, the full evaporation potential is not exploited. To test this hypothesis, we repeat the same analysis using the second model configuration $\Delta T_{\mathrm{mod,obs}}$ that takes into account the actually observed moistening of the air (Fig. 6b). As a consequence, the agreement between observed and modeled cold-pool strength considerably improves ($r = 0.80$, RMSE = 1.3 K). This leads to the conclusion that 64% of the variability in cold-pool strength may be explained by local evaporative cooling in the subcloud layer.

In the previous considerations we have approximated the process of cold-pool formation by moist-adiabatic cooling of the subcloud air mass. However, under these conditions Θ_e would be same inside and outside of the cold pool, which on average is not the case (Fig. 3d). In fact, a negative perturbation in Θ_e indicates the convective import of cooler and drier midtropospheric air into the atmospheric surface layer, which superposes with local evaporative cooling. Since the strength and thermodynamical properties of local downdrafts are highly case dependent, we can treat $\Delta\Theta_e$ as an indicator for the strength of the vertical import of low-Θ_e air into the surface layer. Figure 6c shows the skillfulness of the evaporation model, as quantified by its RMSE, bias, and correlation coefficient with respect to the observed cold-pool strength, as in Figs. 6a and 6b, stratified by observed $\Delta\Theta_e$. For the case of evaporative cooling according to observed moistening, the model RMSE is smallest for small $\Delta\Theta_e$ (0.6 K) and constantly

Brought to you by MAX-PLANCK-INSTITUTE FOR METEOROLOGY | Unauthenticated | Downloaded 04/15/21 07:31 AM UTC

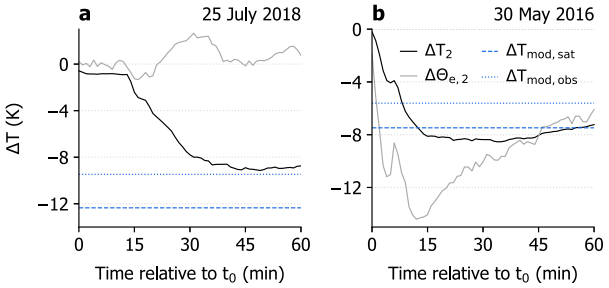

FIG. 7. Time series of observed 2-m temperature perturbation ΔT_2 and equivalent potential temperature perturbation $\Delta\Theta_{e,2}$ during cold-pool events (a) at 1642 LT 25 Jul 2018 and (b) at 1612 LT 30 May 2016. Also indicated are the modeled temperature perturbations $\Delta T_{\mathrm{mod,sat}}$ and $\Delta T_{\mathrm{mod,obs}}$.

increases for increasingly negative $\Delta\Theta_e$ (2.2 K). In cases of large absolute $\Delta\Theta_e$ the model bias is positive indicating an underestimation in cold-pool strength in agreement with the strong vertical advection of low-Θ_e air in such cases. In contrast, for the case of maximum evaporative cooling the model error shows an opposite dependence on $\Delta\Theta_e$, which mainly reflects the previously described overestimation in cold-pool strength that is compensated by increasingly larger $\Delta\Theta_e$. In a sense, the estimated too large evaporative cooling masks the effect of the missing vertical advection of low-Θ_e air, the more so, the stronger the advection.

Despite the simple concepts of the used analysis methods, the presented results provide observational evidence for the generation process of cold pools. Without the convective import of cool and dry upper-level air (i.e., for the 20% of cases with smallest perturbations in Θ_e corresponding to $\Delta\Theta_e > -1.5$ K), local evaporative cooling of the present subcloud layer air by rainfall even explains 92% of the variability in observed near-surface temperature perturbation of a cold pool ($r = 0.96$). Figure 7a shows such a cold-pool event, whose temperature signal is mainly driven by evaporation. In those cases Θ_e is approximately conserved and the observed temperature perturbation agrees well with $\Delta T_{\mathrm{mod,obs}}$. In contrast, for the 20% of cases with largest $\Delta\Theta_e$ (<-5.6 K), the evaporation model fails to reproduce the observed ΔT. For such mainly downdraft-driven cold-pool events the model lacks information about the thermodynamical properties of the advected air mass and underestimates the strength of the observed temperature signal that may even overcompensate the error produced by $\Delta T_{\mathrm{mod,sat}}$ (Fig. 7b). This also becomes manifest in the weak relationship between ΔT and $\Delta\Theta_e$ ($r = 0.37$). Even though evaporative cooling explains the largest part of variability in the temperature signal, only 13% of the observed cold-pool passages are unaffected by convective downdrafts (i.e., $\Delta\Theta_e > -1$ K) and, therefore, entirely evaporation driven. Barnes and Garstang (1982) named a parent rainfall rate of 2 mm h^{-1} as the main criterion for downdrafts to transport upper-level air into the surface layer, still the present data does not show a significant relationship between the maximum observed rainfall rate and $\Delta\Theta_e$ ($r = -0.38$). Another aspect in the interpretation of the results is the cold-pool life cycle stage. Since our analysis does not include the horizontal dimension of the observed cold pools, we miss information on the position of the measurement site relative to the parent convection as well as the cold-pool age. Engerer et al. (2008) and others showed that the local outflow properties considerably vary with the convective life cycle. Therefore, our 13% of entirely evaporation-driven cold pools may also be interpreted as young cold pools, although this needs to be confirmed by further research.

5. Summary and conclusions

In this paper we use multiyear boundary layer mast observations in Hamburg (Germany) to derive an observational reference dataset of the characteristics of convective cold pools. We define a cold-pool event as a 90-min time period that includes a drop in 2-m air temperature of at least 2 K within 20 min in association with local rainfall. For the analyzed 14-yr period between 2006 and 2019 the annual number of observed cold pools varies between 24 and 44 events per summer season, while the monthly number follows an annual cycle with its maximum in July. Furthermore, the average cold-pool activity exhibits a distinct diurnal cycle peaking in the afternoon hours.

Based on the meteorological record we find that the majority of events is associated with a median 2-m temperature perturbation of −3.3 K, while extreme cases reach up to −10.8 K. The constant weakening of the observed temperature signal with height suggests an increased atmospheric stability inside a cold pool compared to its surrounding. For the analyzed events we find an average hydrostatic air pressure rise of 0.7 hPa near the surface with the tendency for a weaker signal above. Consistent with the findings of other studies, the onset of the pressure rise generally precedes the temperature signal by approximately 15 min. By extrapolating the vertical gradient in hydrostatic pressure perturbation for individual cases we estimate a median cold-pool depth of 746 m. According to the perturbation in specific humidity, a cold-pool passage leads to an average moistening of the air by about 1 g kg^{-1}; however, strength and even sign of the signal are highly variable throughout all measurement heights. Also, a clear moisture ring around the cold pool, as generally found in numerical simulations, was not easily recognizable in our observations. Finally, we find significant disturbances of the local wind field, which are increasingly intense away from the surface, expressed by a median horizontal wind speed perturbation of 3.6 (5.3) m s^{-1} at 10 (280)-m height. A distinct and short-lived peak in the vertical wind component minutes prior to the approaching gust front also marks the presence of a lifting-induced circulation ahead of the cold pool.

In the second part of the study we discuss controlling factors of the variability in cold-pool strength to better understand the cold-air production in convective outflows. Observational evidence suggests that contrarily to usual thinking the near-surface temperature perturbation only weakly correlates with the amount of surface rainfall ($r = -0.35$), whereas its statistical relationship with the pre-event saturation deficit is much stronger ($r = -0.71$). To further explore the importance of evaporation for the cold-pool formation, we use a simple

Brought to you by MAX-PLANCK-INSTITUTE FOR METEOROLOGY | Unauthenticated | Downloaded 04/15/21 07:31 AM UTC

thermodynamical model that simulates the wet-bulb cooling process for air of given temperature and humidity. Under the assumption of maximum evaporative cooling, i.e., when saturation is reached, the model is able to reproduce the observed temperature perturbations reasonably well ($r = 0.67$, RMSE = 1.7 K), although it tends to overestimate especially the strength of strong cold pools. The model error considerably decreases, when the evaporative cooling is confined to moistening that corresponds to the maximum observed relative humidity for the respective event ($r = 0.80$, RMSE = 1.3 K). Therefore, we find that local evaporative cooling of subcloud layer air by rainfall explains 64% of the overall variability in cold-pool strength. For cases without considerable import of cooler and drier midtropospheric air by convective downdrafts, indicated by small perturbations of Θ_e, this number even increases to 92%. In contrast, $\Delta\Theta_e$ itself only explains 14% of the observed variance ($r = 0.37$), meaning that the vertical transport of upper-level air masses is a secondary driver for the local temperature signal of a cold pool, which more or less strongly superposes the evaporation process.

Our current understanding of the dynamical and thermodynamical characteristics of cold pools as well as how they interact with their environment is very limited and needs to rely on state-of-the-art convection-resolving simulations. Due to the importance of cold pools for understanding and correctly simulating the organization of convection, the validation of these models requires robust reference data of cold pools. Our work sheds light on the observed properties of continental cold pools over a wider range of meteorological conditions than previous studies have described and identifies processes controlling their signal strength. Nevertheless, current operational networks lack spatial density and sufficient temporal resolution that is vital to observe morphological properties like size, shape, and propagation velocity of cold pools and the submesoscale variability of thermodynamical fields. Our results suggest that future research efforts should focus on the design of observational networks at submesoscale resolution that allow insights into the moisture distributions within cold pools, the interaction with turbulent surface fluxes and the importance of nonhydrostatic pressure effects as an indication of convective downdrafts. This could be achieved using low-budget weather stations and citizen-science approaches. These are essential steps toward a comprehensive understanding of moist convection and its more realistic representation in convection-resolving simulations.

Acknowledgments. This research was carried out in the Hans Ertel Center for Weather Research (HErZ). This German research network of universities, research institutions, and the German Weather Service (DWD) is funded by the BMVI (Federal Ministry of Transport and Digital Infrastructure). The Center for Earth System Research and Sustainability (CEN) and the Max-Planck-Institute for Meteorology support long-term observations at Hamburg Weather Mast. This research contributes to the Cluster of Excellence CLICCS—Climate, Climatic Change, and Society (CLICCS) Topic A3 and A2. We thank Adrian Tompkins and two anonymous reviewers for providing us with helpful comments that improved the quality of the manuscript. Furthermore, we thank Bjorn Stevens for pointing to the importance of Θ_e for this study.

Data availability statement. All observational data and analysis software used during this study are openly available from the long-term archive of the German Climate Computing Center (DKRZ) at http://cera-www.dkrz.de/WDCC/ui/Compact.jsp?acronym=DKRZ_LTA_203_ds00002.

REFERENCES

Barnes, G. M., and M. Garstang, 1982: Subcloud layer energetics of precipitating convection. *Mon. Wea. Rev.*, **110**, 102–117, https://doi.org/10.1175/1520-0493(1982)110<0102:SLEOPC>2.0.CO;2.

Böeing, S. J., H. J. J. Jonker, A. P. Siebesma, and W. W. Grabowski, 2012: Influence of the subcloud layer on the development of a deep convective ensemble. *J. Atmos. Sci.*, **69**, 2682–2698, https://doi.org/10.1175/JAS-D-11-0317.1.

Bolton, D., 1980: The computation of equivalent potential temperature. *Mon. Wea. Rev.*, **108**, 1046–1053, https://doi.org/10.1175/1520-0493(1980)108<1046:TCOEPT>2.0.CO;2.

Brümmer, B., I. Lange, and H. Konow, 2012: Atmospheric boundary layer measurements at the 280 m high Hamburg weather mast 1995–2011: Mean annual and diurnal cycles. *Meteor. Z.*, **21**, 319–335, https://doi.org/10.1127/0941-2948/2012/0338.

Chandra, A. S., P. Zuidema, S. Krueger, A. Kochanski, S. P. de Szoeke, and J. Zhang, 2018: Moisture distributions in tropical cold pools from equatorial Indian Ocean observations and cloud-resolving simulations. *J. Geophys. Res. Atmos.*, **123**, 11 445–11 465, https://doi.org/10.1029/2018JD028634.

De Szoeke, S. P., E. D. Skyllingstad, P. Zuidema, and A. S. Chandra, 2017: Cold pools and their influence on the tropical marine boundary layer. *J. Atmos. Sci.*, **74**, 1149–1168, https://doi.org/10.1175/JAS-D-16-0264.1.

Deutscher Wetterdienst, 2019: DWD Bodenanalyse Archiv. Accessed 8 July 2019, http://www1.wetter3.de/archivdwddt.html.

Engerer, N. A., D. J. Stensrud, and M. C. Coniglio, 2008: Surface characteristics of observed cold pools. *Mon. Wea. Rev.*, **136**, 4839–4849, https://doi.org/10.1175/2008MWR2528.1.

Feng, Z., S. Hagos, A. K. Rowe, C. D. Burleyson, M. N. Martini, and S. P. De Szoeke, 2015: Mechanisms of convective cloud organization by cold pools over tropical warm ocean during the AMIE/DYNAMO field campaign. *J. Adv. Model. Earth Syst.*, **7**, 357–381, https://doi.org/10.1002/2014MS000384.

Fujita, T., 1959: Precipitation and cold air production in mesoscale thunderstorm systems. *J. Meteor.*, **16**, 454–466, https://doi.org/10.1175/1520-0469(1959)016<0454:PACAPI>2.0.CO;2.

Gentine, P., A. Garelli, S.-B. Park, J. Nie, G. Torri, and Z. Kuang, 2016: Role of surface heat fluxes underneath cold pools. *Geophys. Res. Lett.*, **43**, 874–883, https://doi.org/10.1002/2015GL067262.

Goff, R. C., 1976: Vertical structure of thunderstorm outflows. *Mon. Wea. Rev.*, **104**, 1429–1440, https://doi.org/10.1175/1520-0493(1976)104<1429:VSOTO>2.0.CO;2.

Grant, L. D., and S. C. van den Heever, 2016: Cold pool dissipation. *J. Geophys. Res. Atmos.*, **121**, 1138–1155, https://doi.org/10.1002/2015JD023813.

——, and ——, 2018: Cold pool-land surface interactions in a dry continental environment. *J. Adv. Model. Earth Syst.*, **10**, 1513–1526, https://doi.org/10.1029/2018MS001323.

——, T. P. Lane, and S. C. van den Heever, 2018: The role of cold pools in tropical oceanic convective systems. *J. Atmos. Sci.*, **75**, 2615–2634, https://doi.org/10.1175/JAS-D-17-0352.1.

Brought to you by MAX-PLANCK-INSTITUTE FOR METEOROLOGY | Unauthenticated | Downloaded 04/15/21 07:31 AM UTC

Haerter, J. O., and L. Schlemmer, 2018: Intensified cold pool dynamics under stronger surface heating. *Geophys. Res. Lett.*, **45**, 6299–6310, https://doi.org/10.1029/2017GL076874.

Houze, R. A., Jr., 1993: *Cloud Dynamics.* Academic Press, 573 pp.

Khairoutdinov, M., and D. Randall, 2006: High-resolution simulation of shallow-to-deep convection transition over land. *J. Atmos. Sci.*, **63**, 3421–3436, https://doi.org/10.1175/JAS3810.1.

Kirsch, B., 2020: cold_pool_detection version 1.0. Accessed 14 December 2020, https://doi.org/10.5281/zenodo.4321260.

Kurowski, M. J., K. Suselj, W. W. Grabowski, and J. Teixeira, 2018: Shallow-to-deep transition of continental moist convection: Cold pools, surface fluxes, and mesoscale organization. *J. Atmos. Sci.*, **75**, 4071–4090, https://doi.org/10.1175/JAS-D-18-0031.1.

Langhans, W., and D. M. Romps, 2015: The origin of water vapor rings in tropical oceanic cold pools. *Geophys. Res. Lett.*, **42**, 7825–7834, https://doi.org/10.1002/2015GL065623.

Li, Z., P. Zuidema, P. Zhu, and H. Morrison, 2015: The sensitivity of simulated shallow cumulus convection and cold pools to microphysics. *J. Atmos. Sci.*, **72**, 3340–3355, https://doi.org/10.1175/JAS-D-14-0099.1.

Markowski, P., and Y. Richardson, 2010: *Mesoscale Meteorology in Midlatitudes.* Wiley-Blackwell, 407 pp.

Provod, M., J. H. Marsham, D. J. Parker, and C. E. Birch, 2016: A characterization of cold pools in the West African Sahel. *Mon. Wea. Rev.*, **144**, 1923–1934, https://doi.org/10.1175/MWR-D-15-0023.1.

Redl, R., A. H. Fink, and P. Knippertz, 2015: An objective detection method for convective cold pool events and its application to northern Africa. *Mon. Wea. Rev.*, **143**, 5055–5072, https://doi.org/10.1175/MWR-D-15-0223.1.

Rio, C., F. Hourdin, J.-Y. Grandpeix, and J.-P. Lafore, 2009: Shifting the diurnal cycle of parameterized deep convection over land. *Geophys. Res. Lett.*, **36**, L07809, https://doi.org/10.1029/2008GL036779.

Ross, A. N., A. M. Tompkins, and D. J. Parker, 2004: Simple models of the role of surface fluxes in convective cold pool evolution. *J. Atmos. Sci.*, **61**, 1582–1595, https://doi.org/10.1175/1520-0469(2004)061<1582:SMOTRO>2.0.CO;2.

Rotunno, R., J. B. Klemp, and M. L. Weisman, 1988: A theory for strong, long-lived squall lines. *J. Atmos. Sci.*, **45**, 463–485, https://doi.org/10.1175/1520-0469(1988)045<0463:ATFSLL>2.0.CO;2.

Schlemmer, L., and C. Hohenegger, 2014: The formation of wider and deeper clouds as a result of cold-pool dynamics. *J. Atmos. Sci.*, **71**, 2842–2858, https://doi.org/10.1175/JAS-D-13-0170.1.

——, and ——, 2016: Modifications of the atmospheric moisture field as a result of cold-pool dynamics. *Quart. J. Roy. Meteor. Soc.*, **142**, 30–42, https://doi.org/10.1002/qj.2625.

Terai, C. R., and R. Wood, 2013: Aircraft observations of cold pools under marine stratocumulus. *Atmos. Chem. Phys.*, **13**, 9899–9914, https://doi.org/10.5194/acp-13-9899-2013.

Tompkins, A. M., 2001: Organization of tropical convection in low vertical wind shears: The role of cold pools. *J. Atmos. Sci.*, **58**, 1650–1672, https://doi.org/10.1175/1520-0469(2001)058<1650:OOTCIL>2.0.CO;2.

Torri, G., Z. Kuang, and Y. Tian, 2015: Mechanisms for convection triggering by cold pools. *Geophys. Res. Lett.*, **42**, 1943–1950, https://doi.org/10.1002/2015GL063227.

Vogel, R., 2017: The influence of precipitation and convective organization on the structure of the trades. Ph.D. thesis, University of Hamburg, 124 pp.

Zuidema, P., G. Torri, C. Muller, and A. Chandra, 2017: A survey of precipitation-induced atmospheric cold pools over oceans and their interactions with the larger-scale environment. *Surv. Geophys.*, **38**, 1283–1305, https://doi.org/10.1007/s10712-017-9447-x.

Brought to you by MAX-PLANCK-INSTITUTE FOR METEOROLOGY | Unauthenticated | Downloaded 04/15/21 07:31 AM UTC